Chemical Engineering Journal 156 (2010) 512–518

Contents lists available at ScienceDirect

Chemical Engineering Journal

journal homepage: www.elsevier.com/locate/cej

Direct conversion of methane to synthesis gas using lattice oxygen of CeO_2–Fe_2O_3 complex oxides

Kongzhai Li, Hua Wang*, Yonggang Wei, Dongxia Yan

Faculty of Materials and Metallurgy Engineering, Kunming University of Science and Technology, Kunming 650093, China

ARTICLE INFO

Article history:
Received 22 September 2008
Received in revised form 30 March 2009
Accepted 2 April 2009

Keywords:
Methane
CeO_2–Fe_2O_3 complex oxides
Synthesis gas
Gas–solid reaction
Lattice oxygen

ABSTRACT

Three kinds of complex oxides oxygen carriers (CeO_2–Fe_2O_3, CeO_2–ZrO_2 and ZrO_2–Fe_2O_3) were prepared and tested for the gas–solid reaction with methane in the absence of gaseous oxidant. These oxides were prepared by co-precipitation method and characterized by means of XRD, H_2-TPR and Raman. The XRD measurement shows that Fe_2O_3 particles well disperse on ZrO_2 surface and Ce–Zr solid solution forms in CeO_2–ZrO_2 sample. For CeO_2–Fe_2O_3 sample, only a small part of Fe^{3+} has been incorporated into the ceria lattice to form solid solutions and the rest left on the surface of the oxides. Low reduction temperature and low lattice oxygen content are observed over ZrO_2–Fe_2O_3 and CeO_2–ZrO_2 samples, respectively by H_2-TPR experiments. On the other hand, CeO_2–Fe_2O_3 shows a rather high reduction peak ascribed to the consuming of H_2 by bulk CeO_2, indicating high lattice oxygen content in CeO_2–Fe_2O_3 complex oxides. The gas–solid reaction between methane and oxygen carriers are strongly affected by the reaction temperature and higher temperature is benefit to the methane oxidation. ZrO_2–Fe_2O_3 sample shows evident methane combustion during the reducing of Fe_2O_3, and then the methane conversion is strongly enhanced by the reduced Fe species through catalytic cracking of methane. CeO_2–ZrO_2 complex oxides present a high activity for methane oxidation due to the formation of Ce–Zr solid solution, however, the low synthesis gas selectivity due to the high density of surface defects on Ce–Zr–O surface could also be observed. The highly selective synthesis gas (with H_2/CO ratio of 2) can be obtained over CeO_2–Fe_2O_3 oxygen carrier through gas–solid reaction at 800 °C. It is proposed that the dispersed Fe_2O_3 and Ce–Fe solid solution interact to contribute to the generation of synthesis gas. The reduced oxygen carrier could be re-oxidized by air and restored its initial state. The CeO_2–Fe_2O_3 complex oxides maintained very high catalytic activity and structural stability in successive redox cycles. After a long period of successive redox cycles, there could be more solid solutions in the CeO_2–Fe_2O_3 oxygen carrier, and that may be responsible for its favorable successive redox cycles performance.

1. Introduction

The direct conversion of methane to synthesis gas using lattice oxygen of solid oxygen carriers by gas–solid reactions is a novel method for utilization of methane [1]. This process may be achieved in two interconnected reactors. The methane is oxidized by solid oxygen carriers to carbon monoxide and hydrogen in the fuel reactor, and then the reduced oxygen carriers are transferred to the regeneration reactor and re-oxidized by air, water or carbon dioxide. The oxygen carrier is recycled between both reactors in a regenerative process. The synthesis gas with a ratio of H_2/CO = 2 can be obtained successively. Since there is no direct contact between fuels and gaseous molecular oxygen, the risk of explosion can be avoided. Moreover, air can be used instead of pure oxygen, which brings about considerable cost saving when comparing with the technology of partial oxidation of methane (POM) [2]. Further, it is also an attractive technique in environmental protection aspect because the reduced oxygen carriers can be re-oxidized by using carbon dioxide as the oxygen source which is the key factor for the greenhouse effect.

Ceria and the oxide materials containing ceria have attracted much attention as oxidation catalysts for their high activity in the redox reactions and high oxygen storage capacity [3]. The redox properties and the lattice oxygen mobility of CeO_2 can be profoundly enhanced when used in combination with other metal oxides [4]. In fact, the direct use of lattice oxygen of CeO_2-containing materials in selective oxidation of methane has been reported [1,5–7]. However, in these literatures, the reported conversion of methane was still insufficient for practical application, though the synthesis gas could be produced indeed.

In our previous study, a series of CeO_2–Fe_2O_3 complex oxides with varying iron content had been investigated [8]. It showed

* Corresponding author. Tel.: +86 871 5153405.
E-mail address: wanghuaheat@hotmail.com (H. Wang).

1385-8947/$ – see front matter.
doi:10.1016/j.cej.2009.04.038

that the CeO_2–Fe_2O_3 sample with appropriate Fe_2O_3 content (i.e., n_{Ce}:n_{Fe} = 7:3) possessed the best redox properties for selective oxidation of methane to synthesis gas with a H_2/CO ratio of 2 in the absence of molecular oxygen.

In the present work, the CeO_2–Fe_2O_3 complex oxides with a ratio of Ce/Fe = 7/3 was prepared by co-precipitation, and its catalytic activities in the direct conversion of methane to synthesis gas in a fixed-bed reactor were investigated in the absence of gas-phase oxygen. In order to improve the understanding of the roles of Ce and Fe species in the process of methane oxidation by CeO_2–Fe_2O_3 complex oxides, the gas–solid reaction between methane and CeO_2–ZrO_2 or ZrO_2–Fe_2O_3 complex oxides were also investigated. Furthermore, in combination with the characterization methods of Raman, the successive redox cycles performance of CeO_2–Fe_2O_3 oxygen carrier was discussed.

2. Experimental

2.1. Oxygen carrier preparation

CeO_2–Fe_2O_3 complex oxides with a ratio of Ce/Fe = 7/3 were prepared by co-precipitation. The starting materials $Ce(NO_3)_3{\cdot}6H_2O$ and Fe $(NO_3)_3{\cdot}9H_2O$ were mixed according to the mole ratio 7:3, blended in a magnetic stirrer sufficiently and heated at 70 °C. A solution of 10% ammonia was gradually added to the mixture with stirring. When the pH value was increased to 7–8 and 10–11, the resulting solution was maintained at 70 °C with continues stirring for an hour, respectively. The precipitate was filtered and washed with distilled water and ethanol after 2 h settlement. The resulting mixture was dried at 110 °C for 24 h after natural drying overnight and a rufous massive object was obtained. These massive objects were subjected to decomposition at 300 °C for 2 h and grinded into powder. The CeO_2–Fe_2O_3 sample was obtained after these powers calcined under ambient air at 800 °C for 6 h. The CeO_2–ZrO_2 (Ce/Zr = 7:3) or ZrO_2–Fe_2O_3 (Zr/Fe = 7:3) complex oxides were prepared by the same method. The starting material for zirconium oxides was Zr $(NO_3)_4{\cdot}5H_2O$.

2.2. Oxygen carrier characterization

The powders X-ray diffraction (XRD) experiments were performed on a Japan Science D/max-R diffractometer using Cu Ka radiation (λ = 0.15406 nm). The X-ray tube was operated at 40 kV and 40 mA. Data is collected between 2θ = 10–80°.

Temperature programmed reduction (TPR) experiments were performed on TPR Win v 1.50 (produced by Quanta chrome Instruments Co.) under a flow of a 10% H_2/He mixture (75 ml/min) over 100 mg catalysts using a heating rate of 10 °C/min.

The Raman spectra of oxygen carriers were recorded in a Renishaw Invia Raman imaging microscope. The exciting wavelength was 514.5 nm from an Ar ion laser with a power of ca. 4 mW on the samples. The scanning range was 100–1800 cm^{-1}.

The BET surface area was determined by N_2 physisorption using a Quantachrome NOVA 2000e sorption analyzer.

2.3. Oxygen carrier activity tests

2.3.1. Temperature programmed reaction and isothermal reaction

The selective oxidation of CH_4 was carried out in a continuous flow fixed-bed reactor system under atmospheric pressure. An amount of 1.8 g of oxygen carriers was placed in a quartz tube with 19 mm inside diameter. Prior to catalytic reactions, the oxygen carriers were dried in air at 300 °C for 2 h, and then pure N_2 was flowed to the reactor at 400 °C for an hour. The temperature programmed reactions between methane (99.99% purity) and oxygen carriers (CeO_2–Fe_2O_3, CeO_2–ZrO_2 or ZrO_2–Fe_2O_3 sample) were performed in the temperature range of 550–900 °C at a heating rate of 15 °C/min, and the isothermal reaction was performed at 800 °C. The total gas flow rate of the reaction mixture was controlled by a mass flow controller at specific flow rate of 10 ml/min. Reactant and product components were analyzed on line by a gas chromatograph (GC112A, produced by Shanghai Precision & Scientific Instruments Co.). Argon was employed as a carrier gas. CH_4 conversion, CO selectivity and H_2 selectivity was calculated based on the analysis results of GC.

2.3.2. Successive redox cycles

After methane oxidation reaction proceeded for a while, purge pure N_2 for 30 min instead of the CH_4 into the reactor, then introduce the pressed air to regenerate the reduced sample. The reaction proceeds till there are no H_2, CH_4, CO and CO_2. Repeat the preceding steps to evaluate its redox performance. The reaction temperature in this process is 800 °C.

The CH_4 conversion and the selectivity of CO or H_2 were calculated by the following equations:

$$\text{Methane conversion } (\%) = \frac{\text{Moles of methane consumed}}{\text{Moles of methane introduced}} \times 100$$

$$\text{CO selectivity } (\%) = \frac{\text{Moles of CO produced}}{\text{Total moles of CO and } CO_2 \text{ produced}} \times 100$$

$$H_2 \text{ selectivity } (\%) = \frac{\text{Moles of } H_2 \text{ produced}}{\text{Moles of methane introduced} \times 2} \times 100$$

3. Results and discussion

3.1. Oxygen carrier characterization

The XRD results of the fresh CeO_2–Fe_2O_3, CeO_2–ZrO_2 and ZrO_2–Fe_2O_3 oxygen carriers are shown in Fig. 1.

For the CeO_2–Fe_2O_3 sample, the distinct fluorite-type oxide structure of CeO_2 and hexagonal α-Fe_2O_3 could be tested. The main parameter of the ceria lattice was calculated on the basis of the XRD peak of (1 1 1) crystal plane. The lattice parameter of CeO_2 in CeO_2–Fe_2O_3 sample (0.5395 nm) is a little smaller than that of pure CeO_2 (0.5411 nm). It suggests that some small size of Fe^{3+} has been incorporated into the ceria lattice to form the Ce–Fe solid solution resulting in a contraction of the cell parameter [9]. The ZrO_2–Fe_2O_3 sample shows two phases for hexagonal α-Fe_2O_3 and cubic structure of ZrO_2. Comparing with the CeO_2–Fe_2O_3 sample, the intensity of Fe_2O_3 patterns on ZrO_2–Fe_2O_3 is weaker and broader, implying that Fe_2O_3 was better dispersed on ZrO_2 than

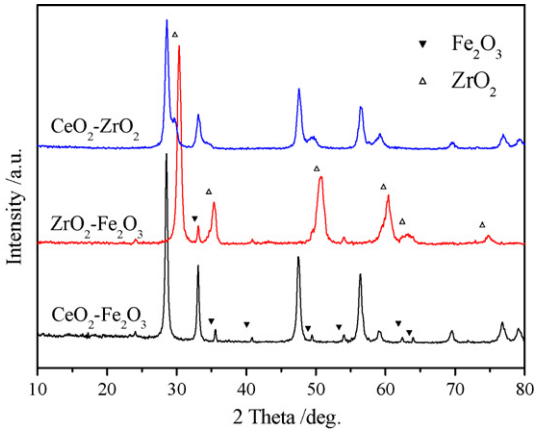

Fig. 1. XRD patterns of CeO_2–Fe_2O_3, CeO_2–ZrO_2 and ZrO_2–Fe_2O_3 oxygen carriers.

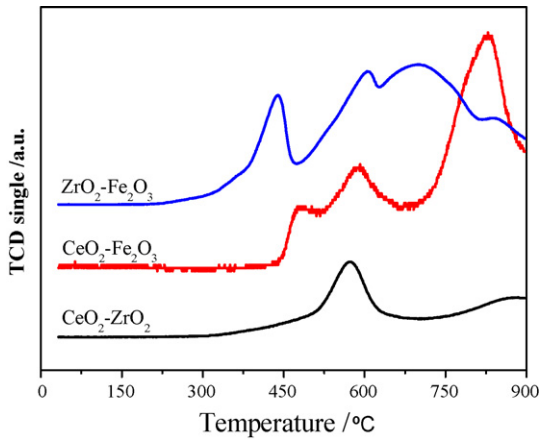

Fig. 2. H_2-TPR profiles of CeO_2–Fe_2O_3, CeO_2–ZrO_2 and ZrO_2–Fe_2O_3 oxygen carriers.

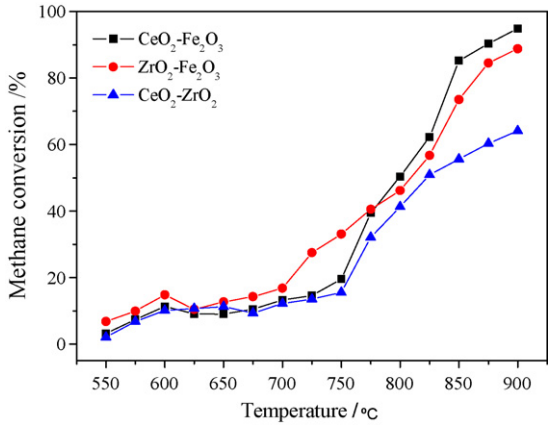

Fig. 3. CH_4 conversion as a function of reaction temperature over CeO_2–Fe_2O_3, CeO_2–ZrO_2 and ZrO_2–Fe_2O_3 oxygen carriers.

on CeO_2 surface. The Fe_2O_3 crystallite size calculated by Scherrer equation is found to be 22.5 nm and the support size of ZrO_2 is 11.3 nm, while the crystallite sizes for Fe_2O_3 and CeO_2 are 33.1 and 19.4 nm, respectively, indicating a better crystallization of those phases in the CeO_2–Fe_2O_3 sample. For the CeO_2–ZrO_2 sample, the characteristic reflections of cubic CeO_2 and rhombohedral ZrO_2 (space group, *R*-3*m*) could be detected. The contraction of the cell parameter (0.5389 nm for CeO_2–ZrO_2 vs 0.5411 nm for pure CeO_2) for CeO_2 indicates the formation of Ce–Zr–O solid solution in the CeO_2–ZrO_2 sample. Furthermore, it could be observed that the peaks of CeO_2–ZrO_2 sample are weaker and broader than those of other two oxygen carriers, indicating that CeO_2–ZrO_2 sample displays the smallest particle size over the three samples.

The H_2-TPR profiles of CeO_2–Fe_2O_3, CeO_2–ZrO_2 and ZrO_2–Fe_2O_3 oxygen carriers are shown in Fig. 2. The CeO_2–ZrO_2 sample features two peaks around 575 °C (major peak) and 875 °C (minor peak). The first peak with a high intensity should be the reduction of the uppermost layers of Ce^{4+}, and the second peak should originate from the reduction of the bulk [10]. This H_2-TPR profile indicates that the surface oxygen is the main oxygen species in the CeO_2–ZrO_2 sample and the bulk oxygen is difficult to be reduced. It is generally accepted [11] that two peaks characterize the two-stage reduction profile of pure Fe_2O_3 ($Fe_2O_3 \rightarrow Fe_3O_4 \rightarrow Fe$). However, the ZrO_2–Fe_2O_3 sample represents three reduction peaks at about 445, 610 and 705 °C, respectively. This phenomenon indicates that there should be an interaction between Fe_2O_3 and its support (ZrO_2) which affects the reduction mechanism of Fe_2O_3 in the ZrO_2–Fe_2O_3 sample. For this reason, the reduction of Fe_2O_3 on the ZrO_2 support may be separated to three steps (i.e., $Fe_2O_3 \rightarrow Fe_3O_4 \rightarrow FeO \rightarrow Fe$), and they are described as three reduction peaks in the H_2-TPR profile. The reduction of CeO_2–Fe_2O_3 also takes place in terms of three obvious peaks at about 490, 610 and 830 °C. According to the H_2-TPR profiles of ZrO_2–Fe_2O_3 and CeO_2–ZrO_2 sample, the three peaks should be ascribed to the reduction of superficial Fe_2O_3, the surface lattice oxygen in CeO_2 or Ce–Fe–O solid solution and the bulk of CeO_2. The overlapping of the first and second reduction peaks indicates that the reduction of surface iron and cerium oxides may occur simultaneously. Since the Fe_2O_3 particles are better dispersed on ZrO_2 than on CeO_2 surface, the first reduction peak for ZrO_2–Fe_2O_3 sample shifts to lower temperature. More importantly, comparing the H_2-TPR profiles of CeO_2–Fe_2O_3 and CeO_2–ZrO_2 sample, the highest intensity of the peak which corresponds to the consuming of H_2 by bulk CeO_2 in CeO_2–Fe_2O_3 sample indicates that the dropped iron species must be benefit to the release of bulk lattice oxygen in CeO_2.

3.2. Gas–solid reaction between CH_4 and oxygen carriers

3.2.1. Temperature programmed reactions

The temperature programmed reactions between methane and different oxygen carriers were performed in a fixed-bed reactor to determine a suitable temperature for the synthesis gas production through gas–solid reaction. The results are reported in terms of CH_4 conversion and the selectivity of desired products (H_2 and CO). Fig. 3 shows the methane conversion as a function of reaction temperature over the different oxygen carriers. The selectivity of CO and H_2 with respect to the reaction temperature is presented in Fig. 4.

As can be seen, methane conversion smoothly begins around 550 °C for all the samples. But the conversion is very low below

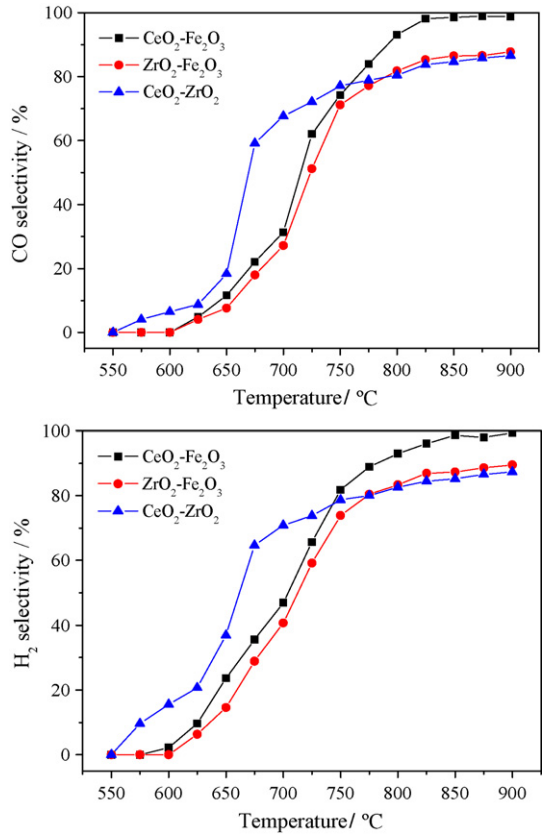

Fig. 4. CO and H_2 selectivity as a function of reaction temperature over CeO_2–Fe_2O_3, CeO_2–ZrO_2 and ZrO_2–Fe_2O_3 oxygen carriers.

700 °C for ZrO_2–Fe_2O_3 and 750 °C for CeO_2–Fe_2O_3 or CeO_2–ZrO_2. Above either temperature, the increase of conversion with T is rapid, which indicates that the methane oxidation by solid oxides is influenced strongly by reaction temperature and a high temperature is necessary for synthesis gas production through gas–solid reaction. This may be due to the rate of oxygen migration from the bulk to the surface increased with rising temperature. We also note a weak peak around 600 °C on the curves of methane conversion for all the materials. Since the surface adsorption oxygen on oxides generally contributes to the oxidation reaction at low temperature [12], this peak may be attributed to the consuming the adsorption oxygen on the oxygen carriers. Among the three samples, ZrO_2–Fe_2O_3 gives the best activity of methane oxidation at low temperature (<775 °C), which is consistent with the lowest reduction temperature observed in Fig. 2 (explained by the well dispersed Fe_2O_3 on the surface of ZrO_2). When the temperature is higher than 775 °C, CeO_2–Fe_2O_3 presents the highest methane conversion. This should be attributed to the well releasing of bulk lattice oxygen in the CeO_2–Fe_2O_3 sample which has been confirmed by the TPR measurement. Similarly, since lower lattice oxygen mobility and less lattice oxygen content towards CeO_2–ZrO_2 sample have been approved in TPR experiment, it shows the lowest conversion through whole test.

From Fig. 4 we can see that the selectivity towards desired products (H_2 and CO) is quite low at the beginning of the temperature programmed reactions, but it increases fast with the temperature rising. Above 800 °C the increase of selectivity with the reaction temperature is slower, but steady. Both the CO and H_2 selectivity reached 93%, 81% and 80% for CeO_2–Fe_2O_3, ZrO_2–Fe_2O_3 and CeO_2–ZrO_2 sample, respectively at 800 °C. Generally, there are two kinds of oxygen species (i.e., surface adsorption oxygen with high activity at low temperature and lattice oxygen with high activity at high temperature) on oxides [12]. Dai et al. [13] reported that methane first reacted with the surface adsorbed oxygen species on $LaFeO_3$ oxides to form CO_2 and H_2O, and then the bulk lattice oxygen can selectively convert methane to CO and H_2 in the absence of gas-phase oxygen. Similarly, Fathi et al. [14] observed that there also were reactive oxygen and weaker oxygen in CeO_2-based oxygen carriers, and the high selectivity towards CO and H_2 could be obtained only when most reactive oxygen had been removed. Therefore, it is reasonable to explain that the low CO and H_2 selectivity at the low temperature can be attributed to the contribution of surface adsorption oxygen on the oxygen carriers. After the surface oxygen declined, the lattice oxygen is responsible for methane selective oxidation into CO and H_2 at high temperature. Furthermore, Sadykov et al. [15] reported that the selectivity for methane oxidation by lattice oxygen also correlated with the density of surface defects on oxygen carrier, and the methane deep oxidation by big part of lattice oxygen was observed due to a high density of surface defects for ceria–zirconia system. This theory gives the reason why CeO_2–ZrO_2 sample shows the lowest CO and H_2 selectivity at high temperature (over 800 °C) in Fig. 4. Moreover, it can be observed that the selectivity towards CO and H_2 both for CeO_2–Fe_2O_3 and ZrO_2–Fe_2O_3 sample are lower than that for CeO_2–ZrO_2 sample below 750 °C. This behavior should be attributed to the appearance of sole Fe_2O_3 species which is suitable to the chemical-looping combustion of methane [16,17]. The fact that CO and H_2 selectivity to ZrO_2–Fe_2O_3 is lower than that to CeO_2–Fe_2O_3 sample throughout the methane oxidation process (showed in Fig. 4) may also be ascribed to above-mentioned characteristic of Fe_2O_3. On the other hand, the lattice oxygen with a high mobility and selectivity which spills from CeO_2 bulk contributes to the selective oxidation of methane with the surface Fe_2O_3 consuming.

The temperature programmed reactions indicate that the selective oxidation of methane to synthesis gas by gas–solid reaction indeed can be achieved at high temperature (≥800 °C), and the lattice oxygen of oxygen carriers is the sole oxidant for the CO and H_2 production. In order to obtain the more detailed data for synthesis gas by gas–solid reaction, the isothermal reactions at 800 °C is investigated.

3.2.2. Isothermal reactions

Fig. 5 represents typical kinetic curves of CH_4 conversion, CO and H_2 selectivity and the ratio of H_2/CO towards the reaction of CH_4 with CeO_2–Fe_2O_3, CeO_2–ZrO_2 and ZrO_2–Fe_2O_3 oxygen carriers, respectively at 800 °C.

For the CeO_2–Fe_2O_3 sample, it shows high methane conversion (over 57%) but low CO and H_2 selectivity (below 46%) at the initial stage. Afterward, there is a sharp decline of methane conversion from 1st to 5th minute, and a quick increase thereafter. On the other hand, a rapid increase towards CO and H_2 selectivity is observed, and then it reaches a steady state level over 91% till 8th minute. It is also can be seen that the ratio of H_2/CO in products approaches to 2 (1.65–2.29) throughout the whole test, especially, the ratio is around 1.95 (1.91–1.99) from 8th to 16th minute. The decline of methane conversion should be attributed to the high consumption rate of surface absorption oxygen or surface Fe_2O_3, while

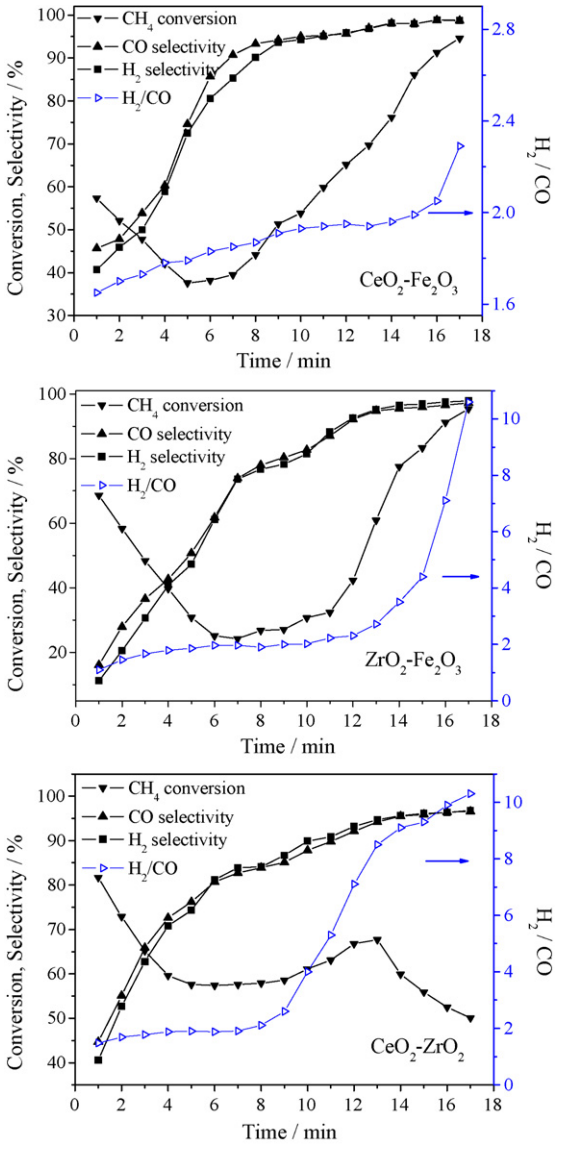

Fig. 5. Catalytic performance for methane oxidation over CeO_2–Fe_2O_3, ZrO_2–Fe_2O_3 and CeO_2–ZrO_2 oxygen carriers at 800 °C.

bulk lattice oxygen in oxygen carrier cannot be timely released to supplement this deficiency. With the surface oxygen species consumed, lattice oxygen is diffused from the bulk to the surface and causes the methane selective oxidation, and this change results in the increase of CO and H_2 selectivity. Our previous study showed that methane could be activated on the metallic Fe surface when the surface Fe_2O_3 had be reduced to original state [8], and the diffusivity of lattice oxygen from CeO_2 bulk to surface can also be enhanced by the appearance of reduced Fe species (known by TPR measurement showed in Fig. 2). Furthermore, with the surface oxygen species consumed, the increased concentration of lattice oxygen vacancies may provide pathways of oxygen transport through the lattice [13]. Therefore, it is rather reasonable that the methane conversion rises rapidly with the reducing of surface Fe_2O_3 or other oxygen species in the present experiment, although the reaction temperature is constant.

The similar trend occurs over ZrO_2–Fe_2O_3 sample. However, a higher methane conversion (over 68%) and lower CO and H_2 selectivity (below 16%) were observed at the initial stage when comparing with the CeO_2–Fe_2O_3 sample, indicating more methane was completely oxidized to CO_2 and H_2O. This phenomenon should be attributed to the better dispersed Fe_2O_3 on ZrO_2 than on CeO_2 (known by XRD measurement showed in Fig. 1). With the oxygen species of Fe_2O_3 consumed, the methane conversion decrease quickly. Since there is only Fe_2O_3 as oxidant in ZrO_2–Fe_2O_3 sample, the posterior increase towards methane conversion due to cracking of methane (with a sharp increase for H_2/CO) is observed in Fig. 5 (ZrO_2–Fe_2O_3). It should be noted that the ratio of H_2/CO in products is around 2.0 (1.86–2.0) from 5th to 9th minute, whereas the CO and H_2 selectivity (47–78%) and methane conversion (27–30%) is low. This phenomenon indicates that the methane selective oxidation and deep oxidation may occur simultaneously when lots of surface lattice oxygen had been consumed, and the activity of bulk oxygen in ZrO_2–Fe_2O_3 is poor for methane oxidation. Through the whole test, low CO and H_2 selectivity at the preliminary stage and excessively high H_2/CO (the maximum reached 10.6) ratio at the later stage confirm poor performance for synthesis gas production over ZrO_2–Fe_2O_3 sample.

The activity towards CeO_2–ZrO_2 sample for methane oxidation is the highest among the three oxygen carriers. The methane conversion reaches 81.7% at the beginning of the reaction, and then declines rapidly to a steady state around 60%. Afterward, an obvious decrease towards methane conversion can be observed. On the other hand, the CO and H_2 selectivity is relatively low comparing with the CeO_2–Fe_2O_3 sample and the ratio of H_2/CO increase quickly over the desired value (i.e. 2.0). The high conversion and low selectivity indicate the reaction was very fast and produced significant quantities of carbon dioxide and water. This fact may be attributed to a high density of surface defects on Ce–Zr–O surface [15] and more oxygen vacancies formed in Ce–Zr solid solution. Since the consuming of lattice oxygen in CeO_2–ZrO_2 sample is very expeditious, the methane decomposition occurs at mid-later period due to the lack of oxygen which results in a rapid increase of the ratio of H_2/CO. Furthermore, the excessive accumulation of carbonaceous on the surface CeO_2–ZrO_2 sample may cover the active sites for the methane decomposition, which would cause the decline of conversion at the later period of reaction.

Obviously, the synthesis gas with the H_2/CO ratio of 2 can be efficiently obtained over CeO_2–Fe_2O_3 oxygen carrier. The ZrO_2–Fe_2O_3 sample shows evident methane combustion during the reducing of Fe_2O_3, and then the methane conversion is strongly enhanced by the reduced Fe species through catalytic cracking of methane. On the other hand, a high activity for methane oxidation is obtained due to the formation of Ce–Zr solid solution, though the low synthesis gas selectivity due to the high density of surface defects on Ce–Zr–O surface can also be observed. Therefore, it is reasonable

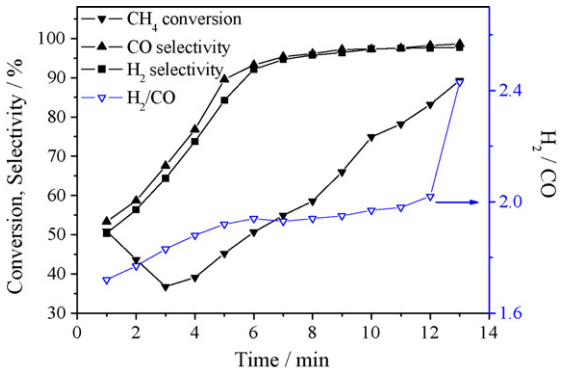

Fig. 6. Catalytic performance for methane oxidation over CeO_2–Fe_2O_3 at fifth redox cycles.

to believe that the good performance for the selective oxidation of methane over CeO_2–Fe_2O_3 oxygen carrier is attributed to the interaction between free Fe species on the CeO_2 surface and Ce–Fe solid solution.

3.3. Successive redox cycles performance

Since the synthesis gas production through gas–solid reaction should be performed in a continuous cycle, the cycle performance for CeO_2–Fe_2O_3 oxygen carrier was also investigated. Successive redox cycles between air and pure methane were carried out in a fixed-bed reactor for the production of synthesis gas over CeO_2–Fe_2O_3 oxygen carrier at 800 °C. The gas flow rates of methane and air were kept at 10 and 30 ml/min, respectively. Pure N_2 was used as dilution gas. Figs. 6 and 7 show the catalytic performance for methane oxidation over CeO_2–Fe_2O_3 at fifth and tenth redox cycles, respectively.

Fig. 6 shows that the CH_4 conversion, CO and H_2 selectivity and the ratio of H_2/CO remain the same trend with the previous description (Fig. 5 (CeO_2–Fe_2O_3)). However, the CO and H_2 selectivity towards the oxygen carrier after five redox cycles is higher than the fresh sample at the early stage of the reaction, indicating the synthesis gas with better selectivity can be obtained through redox cycles. From the 2nd to 12th minute towards the reaction, the ratio of H_2/CO in product is around 2.0 (1.77–2.02). Unfortunately, the ratio of H_2/CO has increased to 2.43 at the 13th minute (Fig. 6), while it just reached 2.05 at the 16th (1.94 at the 13th minute) minute towards the fresh sample (Fig. 5 (CeO_2–Fe_2O_3)). This indicates relatively serious methane decomposition occurred over the CeO_2–Fe_2O_3 oxygen carrier after long-time cycles at higher temperature.

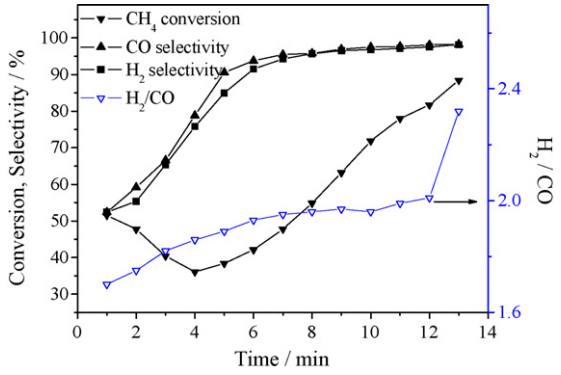

Fig. 7. Catalytic performance for methane oxidation over CeO_2–Fe_2O_3 at tenth redox cycles.

When the cycle number increases to 10, the CH_4 conversion, CO and H_2 selectivity and the ratio of H_2/CO as shown in Fig. 7 present the similar value with the sample after five redox cycles (shown in Fig. 6). From the 5th to 10th redox cycle, there are no higher CO and H_2 selectivity and more serious methane decomposition. This phenomenon indicates that the CeO_2–Fe_2O_3 oxygen carrier can reach a steady state through several redox cycles. We also observed that the surface area towards CeO_2–Fe_2O_3 oxygen carrier declines sharply from 12.56 to 1.74 m^2/g after 10 redox cycles, indicating an obvious sintering occurred over the CeO_2–Fe_2O_3 oxygen carrier after several cycles at higher temperature. It has been reported that the synthesis gas selectivity increased slightly with the surface area of oxygen carrier decreasing [18]. Therefore, the better CO and H_2 selectivity observed in Figs. 6 and 7 should be attributed to the decrease of surface area after redox cycles, and the relatively serious decomposition of methane may be due to the sintering of oxygen carrier.

Fig. 8 shows the laser Raman spectra of the $Ce_{0.7}Fe_{0.3}O_{2-\delta}$ after different treatment. It can be seen that for the fresh sample there are five obviously bands at 216, 280, 460, 570 and 1150 cm^{-1}, respectively. The bands at around 460 and 1150 cm^{-1} are ascribed to the Raman active modes of CeO_2 [19], and the peak located at 216 and 280 cm^{-1} showed the presence of α-Fe_2O_3 [20]. The phonon mode at 570 cm^{-1} is characteristic of oxygen vacancies in the ceria lattice, and this indicates the formation of the solid solution [19]. The Raman spectrums of CeO_2–Fe_2O_3 oxygen carrier after 10 redox cycles is very similar with the fresh sample, indicating CeO_2–Fe_2O_3 oxygen carrier maintained very high structural stability through long-time cycles at high temperature. Moreover, it is worth to mention that there is a small shift of the bands at 460 cm^{-1} to lower frequencies because of the successive redox cycles (shown in Fig. 8 insert). Generally, the incorporation of other metal ion into the ceria lattices to form solid solution can result in the shifts of this band position [19]. Therefore, it can be pointed out that there should form more solid solutions in the CeO_2–Fe_2O_3 oxygen carrier after a long period of successive redox cycles, and this may counterbalances the unfavorable influence caused by the sintering of oxygen carrier and obtain a relatively high methane conversion to some extent.

Obviously, the CeO_2–Fe_2O_3 oxygen carrier exhibits satisfactory successive redox cycles performance for the synthesis gas production. The successive redox cycles result in a sintering for the oxygen carrier which may cause premature decomposition of methane, however, the low surface area is favorable to enhance the selective oxidation ability of oxygen carrier. On the other hand, more Ce–Fe solid solution formations are observed through several cycles, which may benefit the continuous production of synthesis gas production over CeO_2–Fe_2O_3 oxygen carrier.

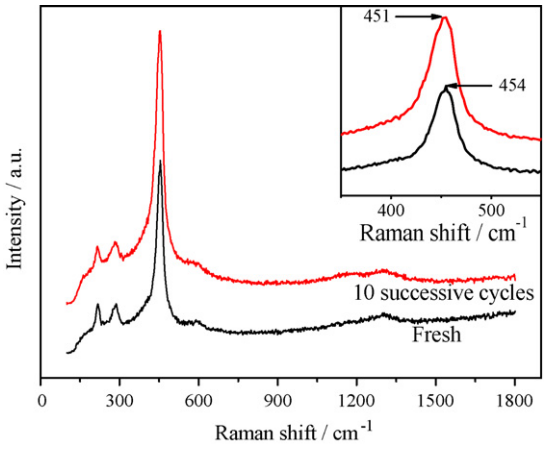

Fig. 8. Comparison of Raman spectra over fresh and after 10 successive redox cycles CeO_2–Fe_2O_3 oxygen carrier.

4. Conclusions

Direct conversion of methane to synthesis gas using lattice oxygen of solid complex oxides (i.e., CeO_2–Fe_2O_3, CeO_2–ZrO_2 and ZrO_2–Fe_2O_3) is reported. The temperature programmed reactions show that both the methane conversion and the selectivity towards CO and H_2 are strongly affected by the reaction temperature and they increase rapidly with rising temperature, which should be attributed to high rate of lattice oxygen migration under high temperature. The isothermal reactions at 800 °C indicate that the selective oxidation of methane to synthesis gas by gas–solid reaction depends not only on the features of activated oxygen species (i.e., lattice oxygen) but on the route of methane activation (i.e., on reduced Fe species) and the lattice oxygen mobility, similarly with the proposal by Sadykov et al. [15].

The Fe_2O_3 dispersed on ZrO_2 surface is suitable for methane combustion, and the methane can be activated by reduced Fe species due to its catalytic performance for methane decomposition. A high release rate of lattice oxygen is observed over CeO_2–ZrO_2 complex oxides because of the formation of Ce–Zr solid solution; however, it presents the low synthesis gas selectivity in virtue of the high density of surface defects on Ce–Zr–O surface. On the other hand, CeO_2–Fe_2O_3 oxygen carrier shows high activity and selectivity for the synthesis gas production and satisfactory stability in redox cycles. The interaction between dispersed Fe_2O_3 on the surface of CeO_2 and Ce–Fe solid solution should contribute to this favorable performance.

Acknowledgements

Supported by the National Nature Science Foundation of China (No. 50574046, No. 50774038) and National Natural Science Foundation of Major Research Projects (No. 90610035), High School Doctoral Subject Special Science and Research Foundation of Ministry of Education (No. 20040674005).

References

[1] K. Otsuka, T. Ushiyama, I. Yamanaka, Partial oxidation of methane using the redox of cerium oxide, Chem. Lett. 22 (1993) 1517–1520.
[2] E.R. Stobbe, B.A. Boer, J.W. Geus, The reduction and oxidation behaviour of manganese oxides, Catal. Today 47 (1999) 161–167.
[3] N. Laosiripojana, D. Chadwick, S. Assabumrungrat, Effect of high surface area CeO_2 and Ce–ZrO_2 supports over Ni catalyst on CH_4 reforming with H_2O in the presence of O_2, H_2, and CO_2, Chem. Eng. J. 138 (2008) 264–273.
[4] P. Vidmar, P. Fornasiero, J. Kaspar, Effects of trivalent dopants on the redox properties of $Ce_{0.6}Zr_{0.4}O_2$ mixed oxide, J. Catal. 171 (1997) 160–168.
[5] K. Otsuka, Y. Wang, M. Nakamura, Direct conversion of methane to synthesis gas through gas–solid reaction using CeO_2–ZrO_2 solid solution at moderate temperature, Appl. Catal. A Gen. 183 (1999) 317–324.
[6] K. Otsuka, Y. Wang, E. Sunada, I. Yamanaka, Direct partial oxidation of methane to synthesis gas by cerium oxide, J. Catal. 175 (1998) 152–160.
[7] Y.G. Wei, H. Wang, K.Z. Li, M.C. Liu, Preparation and performance of Ce/Zr mixed oxides for direct conversion of methane to syngas, J. Rare Earths 25 (2007) 110–114.
[8] K.Z. Li, H. Wang, Y.G. Wei, M.C. Liu, Preparation and characterization of $Ce_{1-x}Fe_xO_2$ complex oxides and its catalytic activity for methane selective oxidation, J. Rare Earths 26 (2008) 245–249.
[9] F.J. Pérez-Alonso, M. López Granados, M. Ojeda, P. Terreros, S. Rojas, T. Herranz, J.L.G. Fierro, Chemical structures of coprecipitated Fe–Ce mixed oxides, Chem. Mater. 17 (2005) 2329–2339.
[10] I. Atribak, A. Bueno-López, A. García-García, Combined removal of diesel soot particulates and NO_x over CeO_2–ZrO_2 mixed oxides, J. Catal. 259 (2008) 123–132.
[11] G. Magnacca, G. Cerrato, C. Morterra, M. Signoretto, F. Somma, F. Pinna, Structural and surface characterization of pure and sulfated iron oxides, Chem. Mater. 15 (2003) 675–687.
[12] E.J. Baran, Structural chemistry and physicochemical properties of perovskite-like materials, Catal. Today 8 (1990) 133–151.

[13] X.P. Dai, R.J. Li, C.C. Yu, Z.P. Hao, Unsteady-state direct partial oxidation of methane to synthesis gas in a fixed-bed reactor using $AFeO_3$ (A = La, Nd, Eu) perovskite-type oxides as oxygen storage, J. Phys. Chem. B 110 (2006) 22525–22531.
[14] M. Fathi, E. Bjorgum, T. Viig, O.A. Rokstad, Partial oxidation of methane to synthesis gas: elimination of gas phase oxygen, Catal. Today 63 (2000) 489–497.
[15] V.A. Sadykov, T.G. Kuznetsova, G.M. Alikina, Y.V. Frolova, A.I. Lukashevich, Y.V. Potapova, V.S. Muzykantov, V.A. Rogov, V.V. Kriventsov, D.I. Kochubei, E.M. Moroz, D.I. Zyuzin, V.I. Zaikovskii, V.N. Kolomiichuk, E.A. Paukshtis, E.B. Burgina, V.V. Zyryanov, N.F. Uvarov, S. Neophytides, E. Kemnitz, Ceria-based fluorite-like oxide solid solutions as catalysts of methane selective oxidation into syngas by the lattice oxygen: synthesis, characterization and performance, Catal. Today 93–95 (2004) 45–53.
[16] T. Mattission, A. Lyngfelt, P. Cho, The use of iron oxide as an oxygen carrier in chemical-looping combustion of methane with inherent separation of CO_2, Fuel 80 (2001) 1953–1962.
[17] A. Abad, T. Mattisson, A. Lyngfelt, M. Johansson, The use of iron oxide as oxygen carrier in a chemical-looping reactor, Fuel 86 (2007) 1021–1035.
[18] X.P. Dai, C.C. Yu, R.J. Li, Q. Wu, K.J. Shi, Z.P. Hao, Effect of calcination temperature and reaction conditions on methane partial oxidation using lanthanum-based perovskite as oxygen donor, J. Rare Earths 26 (2008) 341–346.
[19] J.R. Mcbride, K.C. Hass, B.D. Poindexter, Raman and X-ray studies of $Ce_{1-x}RE_xO_{2-y}$, where RE = La, Pr, Nd, Eu, Gd and Tb, J. Appl. Phys. 76 (1994) 2435–2441.
[20] D.L.A. De Faria, S. Venaü ncio Silva, M.T. De Oliveira, Raman microspectroscopy of some iron oxides and oxyhydroxides, J. Raman Spectrosc. 28 (1997) 873–878.